



## Adsorptive removal of diuron on biomass ashes: a comparative study using rice husk ash and bagasse fly ash as adsorbents

Sunil K. Deokar<sup>a</sup>, Diksha Singh<sup>a</sup>, Sweta Modak<sup>a</sup>, Sachin A. Mandavgane<sup>a,\*</sup>,  
Bhaskar D. Kulkarni<sup>b</sup>

<sup>a</sup>Department of Chemical Engineering, VNIT, Nagpur 440010, India, Tel. +91 712 2801563; Fax: +91 712 2223969; emails: sam@che.vnit.ac.in, mandavgane1@gmail.com (S.A. Mandavgane)

<sup>b</sup>CSIR-National Chemical Laboratory, Pune 411 008, India

Received 20 August 2015; Accepted 5 December 2015

### ABSTRACT

This study describes the use of two types of biomass ashes (BMAs) as adsorbents for diuron removal. Two BMAs, namely rice husk ash (RHA) and bagasse fly ash (BFA), were used in this study, and their adsorption behavior and adsorption mechanism were compared based on various characteristics, such as surface area, pore diameter, and volume. It was found that the particle size and the composition of these BMAs, especially the content of carbon and silica, primarily affect the adsorption kinetics and capacity. Compared with RHA, BFA has more carbon content (47.37%), and therefore shows higher adsorption capacity (43.48  $\mu\text{mol/g}$ ). In addition, BFA has larger external surface area and exhibited faster kinetics at the initial adsorption stage; by contrast, RHA due to its larger pore diameter allows for faster pore adsorption and surpasses the initial kinetic rate of BFA. For the same particle size (0.354–0.251 mm), the equilibrium capacity of BFA was found to be four times greater than that of RHA; in addition, the surface area of BFA is two times more than that of RHA, suggesting that BFA has more active sites than RHA. It was found that solution pH influences adsorption mechanism of diuron molecule on BMA. The uptake capacity of BFA and RHA is 10 times greater than natural adsorbents such as soil and is comparable with synthetic adsorbents such as activated carbon and multiwalled carbon nanotubes. To our knowledge, removal of diuron using ashes has not been reported previously.

*Keywords:* Adsorption; Bagasse fly ash; Biomass ash; Diuron; Rice husk ash

### 1. Introduction

Rice husk and bagasse are two of the most common globally produced biomass materials, which are used as solid fuel in both domestic and industrial applications. Based on the production of rice and sugarcane [1], approximately 23 million tons of rice husk and 89 million tons of bagasse were produced in

2012–2013, which on combustion generated 6 million tons of rice husk ash (RHA) and 2 million tons of bagasse fly ash (BFA), respectively [2,3]. RHA and BFA are commonly referred to as biomass ashes (BMAs). Because these BMAs are produced in large quantities, they should be reused to avoid disposal problem. In the recent past, there is a growing interest to explore the use of BMA for different applications. At present, RHA is widely exploited in construction

\*Corresponding author.

field to prepare high-strength concrete, refractory bricks, and as a feedstock for processing industries in addition to being a characteristic improviser in the production of polymers and composites [4]. RHA as an effective adsorbent for the removal of heavy metals, dyes, phenols, and inorganic anions has been reported previously [5]. Compared with RHA, BFA only has limited utilization in cement and concrete production owing to its higher carbon content. However, several studies have shown that BFA is an economically viable adsorbent for the removal of metal ions, dyes, and organic compounds (e.g. phenols) [6]. The capability of BMA to remove pesticide from aqueous solution has not been examined in detail, except for the use of BFA to remove lindane and malathion from aqueous solution [7]. This study is an attempt to explore BMA as an adsorbent for pesticide removal and to establish the relationship between BMA characteristics and its adsorption efficacy using diuron as the representative adsorbate.

Diuron, a nonselective postemergence urea herbicide, is used worldwide to control broadleaf and grassy weeds. As a result, increasingly higher concentrations of diuron are detected in surface and groundwater because of its high chemical stability and leaching potential [8,9]. In most cases, pesticide removal is achieved by adsorption because it is better in terms of cost, operation, and efficiency than other methods. The adsorbents used in the past for diuron adsorption primarily include activated carbon, polymers, carbon nanotubes, soils, and clays [10–16]. To our knowledge, removal of diuron using ashes is not reported yet, and this study focuses on the use of BMA for adsorption of diuron from aqueous solution for the first time. The advantages of this method include the availability of large amounts of BMA and low cost.

The aim of this study was to evaluate and compare diuron removal capacity of RHA and BFA by studying the effect of various parameters such as adsorbent dosages, adsorbate concentration, contact time, pH, particle size of adsorbents, and temperature.

## 2. Materials and methods

### 2.1. Adsorbents

RHA and BFA were supplied by M/s Yash Agro Ltd, Nagpur (India) and M/s Wainganga Sugar and Power Ltd. Bhandara (India), respectively. Bagasse and rice husk were used as fuel for boiler in these industries. Proximate analysis of BMA was performed according to a standard method [17]. The surface characteristics, namely surface area, pore diameter, and volume were measured using Micromeritics ASAP

2010 instrument. The chemical composition of BMA was investigated with an XRF analyzer (PW 2403; PANalytical). The compositions of carbon, hydrogen, nitrogen, and sulfur in BMA were determined with an elemental analyzer (vario MACRO Cube; Elementar, Hanau, Germany).

### 2.2. Adsorbate

The adsorbate diuron (98%) was purchased from Sigma-Aldrich and used without any additional treatment. The physicochemical properties of diuron are listed in Table 1. The stock solution was prepared by dissolving an accurately weighted amount of diuron in deionized water, and the solution was diluted successively according to experimental runs.

### 2.3. Batch adsorption

In the batch adsorption study, glass vials containing 25 mL diuron solution were agitated in a constant-temperature water-bath shaker after adding a predefined quantity of BMA. Samples withdrawn after appropriate treatment time were filtered and residual concentration after centrifugation was determined on a UV-vis spectrophotometer (Model UV 1800; Shimadzu, Japan) at 248 nm. The percentage removal and adsorption capacity ( $q_t$  and  $q_e$  mg/g) at any time and at equilibrium were calculated as follows:

$$\% \text{ Removal} = \left( \frac{C_0 - C_e}{C_0} \right) \times 100 \quad (1)$$

$$q_t = \frac{(C_0 - C_t)V}{W} \quad (2)$$

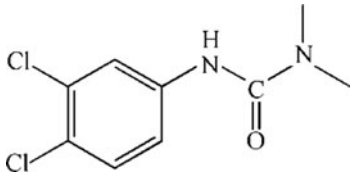
$$q_e = \frac{(C_0 - C_e)V}{W} \quad (3)$$

where  $C_0$  ( $\mu\text{mol/L}$ ) and  $C_e$  ( $\mu\text{mol/L}$ ) are the initial and equilibrium concentrations of diuron, respectively.  $V$  (L) is volume of the solution and  $W$  (g) is adsorbent mass. The effect of adsorbent dosage, initial concentration, contact time, pH, and temperature on adsorption of diuron was studied. Each experiment was carried out in triplicates under identical conditions and the average value was reported.

### 2.4. Adsorption modeling: kinetic and isotherm

The potential of an adsorbent is evaluated based on its capacity, adsorption rate, mechanical strength, and the probability of regeneration and reuse.

Table 1  
Chemical structure and physicochemical properties of diuron

Properties	Diuron
Structure	
Molecular formula	C <sub>9</sub> H <sub>10</sub> Cl <sub>2</sub> N <sub>2</sub> O
Molecular weight (g/mol)	233.09
Solubility in water at 25°C (mg/L)	42
Dipolar moment (Debyes)	7.55
Density (cm <sup>3</sup> /g)	1.1786

Adsorbent capacity is mainly calculated from isotherm models applied to equilibrium data. The parameters and fundamental thermodynamic assumptions of isotherm models provide insight into surface properties, adsorbent affinity, and adsorption mechanism. Few commonly used isotherms models are Langmuir, Freundlich, and Temkin [18] and these are applied in this article. Adsorption kinetics is important to investigate the rate-controlling step as well as the underlying mechanism. Pseudo-first-order (PFO), pseudo-second-order (PSO), intraparticle diffusion (IPD), and Elovich (EL) [19] are the most commonly applied kinetic models. The linearized form of the isotherm and kinetic models along with their plots, slopes, and intercepts are listed in Table 2. The model constants are calculated from slopes and intercepts of the linearized form of models. Statistical analysis between experimental results and results predicted by models (isotherms

and kinetic) is done using some functions. The commonly applied statistical functions, which include average relative errors (ARE, %), the sum of the squares of the error (SSE) and Marquardt's percent standard deviation (MPSD), are given in supplementary information.

### 2.5. Thermodynamic properties

The thermodynamic properties (both directly and indirectly measurable) such as equilibrium constant, temperature, enthalpy, entropy, and Gibbs free energy are essential for accurate designing of any adsorption system. In addition, these properties are important to check viability, spontaneity, and nature of adsorption process, and are determined using thermodynamic relations [20]. In this study, changes in enthalpy ( $\Delta H$ ), entropy ( $\Delta S$ ), and Gibbs free energy ( $\Delta G$ ) were

Table 2  
Details of kinetic and isotherm models applied for adsorption of diuron on BMA

	Linearized form	Plot	Slope	Intercept
<i>Kinetic models</i>				
Pseudo-first-order	$\ln(q_e - q_t) = \ln q_e - k_1 t$	$\ln(q_e - q_t) : vs : t$	$-k_1$	$\ln q_e$
Pseudo-second-order	$\frac{t}{q_t} = \frac{1}{k_2 q_e^2} + \frac{t}{q_e}$	$\frac{t}{q_t} : vs : t$	$\frac{1}{q_e}$	$\frac{1}{k_2 q_e^2}$
Elovich	$q_t = \frac{1}{\beta} \ln(\alpha\beta) + \frac{1}{\beta} \ln t$	$q_t : vs : \ln t$	$\frac{1}{\beta}$	$\frac{\ln(\alpha\beta)}{\beta}$
Intraparticle diffusion	$q_t = k_d t^{1/2} + C$	$q_t : vs : t^{1/2}$	$k_d$	$C$
<i>Isotherm models</i>				
Langmuir	$\frac{C_e}{q_e} = \frac{1}{K_L q_{max}} + \frac{C_e}{q_{max}}$	$\frac{C_e}{q_e} : vs : C_e$	$\frac{1}{K_L q_{max}}$	
Freundlich	$\log q_e = \log K_F + \frac{1}{n} \log C_e$	$\log q_e : vs : \log C_e$	$\frac{1}{n}$	$\log K_F$
Temkin	$q_e = B \ln A_T + B \ln C_e$ $B = \frac{RT}{b_T}$	$q_e : vs : \ln C_e$	$B$	$B \ln A_T$

investigated by applying Eqs. (4) and (5) to experimental findings obtained at different temperatures and initial concentrations:

$$\ln K_p = -\frac{\Delta H}{RT} + \frac{\Delta S}{R} \quad (4)$$

$$\Delta G = -RT \ln K_p \quad (5)$$

where  $K_p$  the thermodynamic equilibrium constant is the ratio of equilibrium concentration of adsorbate in the solid and liquid phases. The values of  $\Delta H$  and  $\Delta S$  were derived from the slope and intercept of linear plot (i.e. van't Hoff plot) of  $\ln K_p$  vs.  $1/T$ , respectively.

### 3. Results and discussion

#### 3.1. Characterization of BMA

The moisture, volatile matter, ash, and fixed carbon content were found to be 1.80, 6.16, 89.87, and 2.14% in RHA whereas 6.30, 42.46, 40.16, and 11.10% in BFA, respectively. The percentage of carbon identified by CHNS analysis of RHA and BFA was 5.85 and 47.37, respectively, whereas silica content determined by XRF analysis was 81.78 and 36.14%, respectively. BMA consists of trace quantities of metal oxides which play an important role in the adsorption process by forming charges on the surface of BMA in aqueous solution. The few metal oxides present in RHA and BFA are given Table 3 which shows more content of  $Al_2O_3$  in RHA and  $CaO$  in BFA. Density of RHA having average particle size  $144 \mu m$  is found to be  $0.258 g/cm^3$  while that of BFA having average particle size  $118 \mu m$  is  $0.212 g/cm^3$ . The BET surface area of BFA ( $51.93 m^2/g$ ) is greater than that of RHA ( $33.99 m^2/g$ ), which suggests the dominance of carbon over silica in providing higher surface area in the case of BFA. The micropore area of BFA and RHA is  $13.67$  and  $5.67 m^2/g$ , respectively. The external surface area, calculated from BET surface area and micropore area, is found to be  $38.26$  and  $28.32 m^2/g$  for BFA and RHA, respectively. The pore volume and pore diameter of BFA and RHA were  $4.96 \times 10^{-2}$  and

$2.69 \times 10^{-3} cm^3/g$  and  $45.577$  and  $80.60 \text{ \AA}$ , respectively, which suggests the existence of deeper pores on BFA and shallower pores on RHA surfaces.

The scanning electron micrographs of RHA and BFA are previously described [21] and reveal the presence of particles of different sizes in both ashes. The aspect ratios in the range of 2.6:1–4.4:1 for BFA and 2.4:1–4.8:1 for RHA are earlier reported.

#### 3.2. Effect of BMA dosage

The increase in diuron uptake with dosage was observed by varying the dosage of RHA and BFA in the range of 0.05–0.5 and 0.01–0.15 g/25 mL solution, respectively, for a fixed time (16 h) and concentration ( $85.84 \mu mol/L$ ). From Fig. 1, it can be seen that significantly higher removal was achieved on BFA than on RHA. This can be attributed to the higher BET surface area and carbon composition in BFA. Almost 90% removal was achieved using 0.25 g RHA and 0.06 g BFA, and no significant removal was observed for dosages beyond this range; therefore, these were chosen as optimal dosages for further studies.

#### 3.3. Effect of initial concentration

The effect of initial concentration of diuron on percentage removal was studied by varying the concentration from 21.46 to  $128.76 \mu mol/L$ . The results presented in Fig. 2 demonstrate the reduction in percentage removal with the increase in concentration. Because BMAs have a finite number of adsorption sites, percentage removal is considerably decreased at higher concentrations [22]. However, equilibrium capacity is increased due to mass-transfer resistance, which is overcome by greater driving force at higher concentrations [22]. The equilibrium capacities of BMA are increased by approximately by fivefold when the concentration is increased from 21.46 to  $128.76 \mu mol/L$ . This increase in equilibrium capacity with respect to concentration is higher for BFA than for RHA and it is due to higher surface area of BFA which offers more adsorption sites.

Table 3  
Chemical composition of RHA and BFA

	$Al_2O_3$ %	$K_2O$ %	$Fe_2O_3$ %	$CaO$ %	$MgO$ %	$Na_2O$ %	$P_2O_5$ %	$MnO$ %	$TiO_2$ %	$CuO$ %
RHA	4.08	1.87	1.27	1.27	0.50	0.19	0.78	0.12	0.40	0.008
BFA	1.10	2.32	1.62	3.10	1.86	1.20	3.05	1.15	1.22	0.12

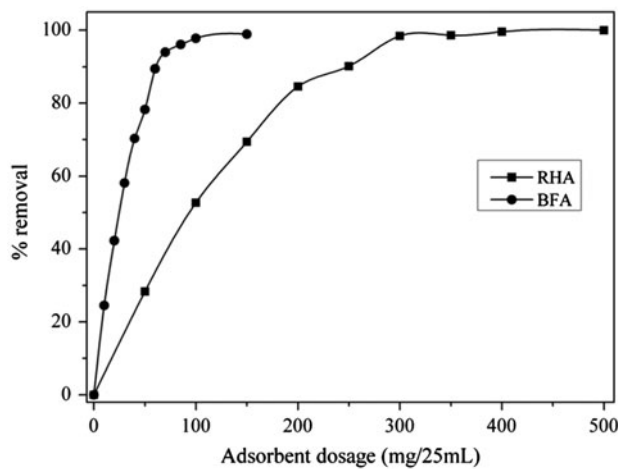


Fig. 1. Effect of RHA and BFA dosage on the removal of diuron ( $C_0 = 85.84 \mu\text{mol/L}$ ).

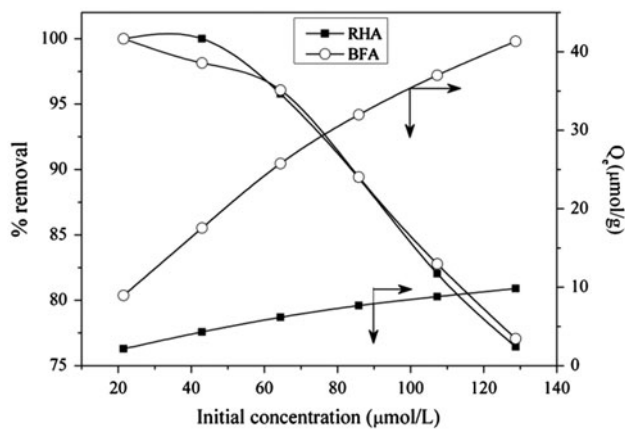


Fig. 2. Effect of initial concentration on the removal of diuron using 0.25 g RHA and 0.06 g BFA per 25 mL.

### 3.4. Effect of contact time

To compare equilibrium times at different concentrations, the adsorption of diuron on both types of ashes was performed as a function of contact time. The percentage removal is initially higher on BFA, but after 60 min for  $42.92 \mu\text{mol/L}$  and 70 min for  $85.84, 128.76 \mu\text{mol/L}$ , it is higher on RHA as presented in Fig. 3 and also in Table 4. This phenomenon can be explained with the help of external surface area and pore diameter. The initial uptake is higher on BFA due to its higher external surface area as discussed in "Characterization of BMA" section. However, after 60–70 min, the uptake is higher on RHA owing to its larger pore diameter. Because of the presence of deeper pores and higher BET surface area, BFA has the higher overall equilibrium time and thus, higher

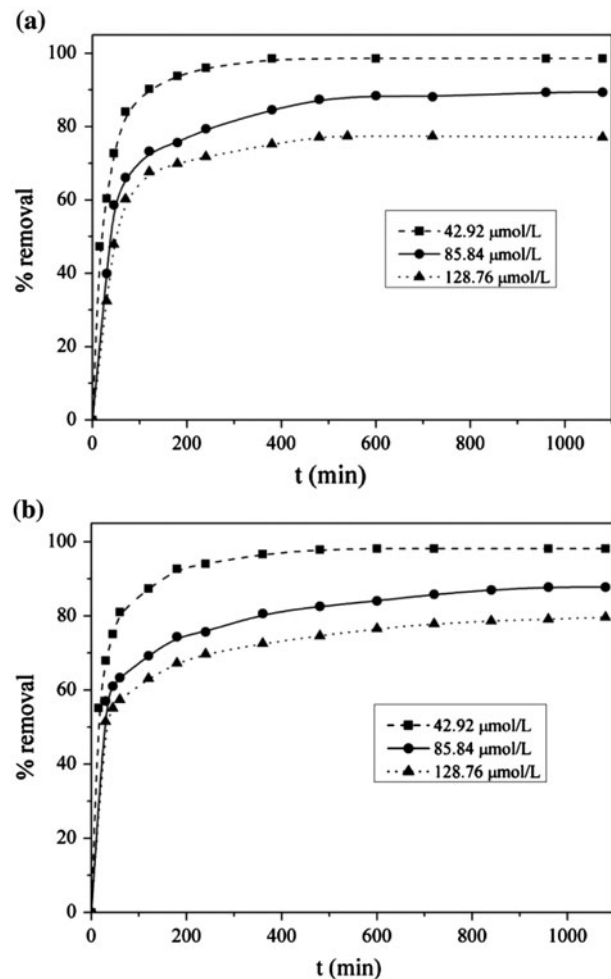


Fig. 3. Effect of contact time on the removal of diuron using (a) RHA-0.25 g and (b) BFA-0.06 g per 25 mL.

adsorption capacity. It can be deduced that the equilibrium capacity and time are about four-order and two-order higher, respectively, when the carbon content is eight-order higher in BFA than in RHA.

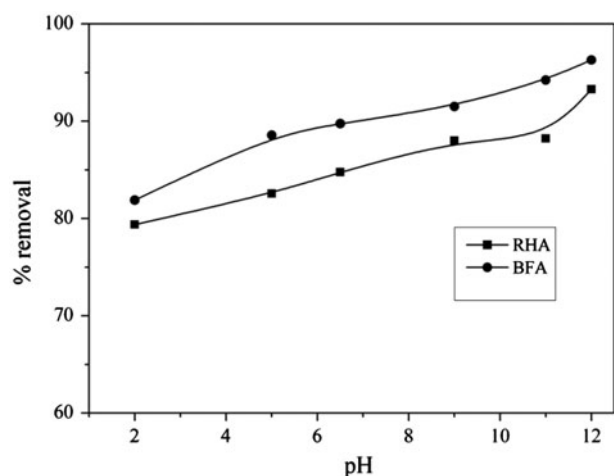
### 3.4. Effect of pH

Because both surface charge of adsorbent and degree of ionization of adsorbate are dependent on pH, the effect of solution pH on adsorption behavior of BMA was studied by varying the pH between 2 and 12. The percentage removal, shown in Fig. 4, for  $85.84 \mu\text{mol/L}$  concentration is proportional to pH, and this tendency can be explained as follows: Camara et al. [23] found that diuron acts as a neutral molecule at pH above 6, but as cationic species at pH below 6. The surface of BMA develops positive charges when solution pH is less than point of zero charge ( $\text{pH}_{\text{pzc}}$ );

Table 4

Percentage removal in initial part and later part of adsorption of diuron on RHA and BFA

$C_0$ ( $\mu\text{mol/L}$ )	$t$ (min)	% Removal		$C_0$ ( $\mu\text{mol/L}$ )	$t$ (min)	% Removal		$C_0$ ( $\mu\text{mol/L}$ )	$t$ (min)	% Removal	
		RHA	BFA			RHA	BFA			RHA	BFA
42.92	15	47.30	55.16	85.84	30	39.94	57.04	128.76	30	32.45	51.51
	30	60.39	67.96		45	58.63	61.03		45	47.91	55.07
	45	72.72	75.12		70	66.14	63.34		70	60.25	57.38
	60	84.04	81.03		120	73.24	69.26		120	67.65	63.12
	120	90.24	87.36		180	77.11	72.91		180	70.22	66.71

Fig. 4. Effect of pH on the removal of diuron ( $C_0 = 85.84 \mu\text{mol/L}$ ).

however, when  $\text{pH} > \text{pH}_{\text{pzc}}$ , negative charges are formed. The  $\text{pH}_{\text{pzc}}$  of both ashes studied is in the range of 8–9 [24,25]; at lower pH, electrostatic repulsive interactions occur between the positive BMA surface and the cationic diuron. Around pH 7, nonelectrostatic interactions between diuron and BMA result in slight improvement in adsorption capacity as the system becomes electrostatically neutral. At higher pH, however, where diuron molecules are neutral and the adsorbent surface is negative, nonelectrostatic interactions are predominant, subsequently leading to considerable increase in diuron removal [23].

### 3.5. Effect of particle size of BMA

RHA and BFA were sieved using BSS into different size fractions as shown in Table 5, and the size fractions were shaken with diuron ( $85.84 \mu\text{mol/L}$ ) for 16 h. Previous studies have reported higher removal due to the larger surface area available for smaller size particles [26,27]. However, this study indicates higher removal of diuron for large-sized particles of BMA, as

indicated in Fig. 5. Characteristics of the particle-size ranges mentioned in Table 5 indicate that the BET surface area increases and the silica-to-carbon ratio decreases with the increase in particle size. The plausible reasons for lesser BET surface area for smaller particles may be blocking of pores (mesopores/macropores) by submicrometer-scale particles [28] and also nonporous fines may be present in BMA, which predominantly ended up as smaller particle-size fractions [29]. The equilibrium capacity for 0.354–0.251-mm particle size of RHA and BFA was found to be 7.89 and  $34.42 \mu\text{mol/g}$ , respectively. Thus, the equilibrium capacity for this particle size of BFA is about four times that of RHA, whereas the BET surface area for the aforementioned particle size of BFA is nearly double than that of RHA. Thus, the BFA surface has more active sites in addition to surface area, which are responsible for its higher adsorption capacity, compared with RHA.

### 3.6. Effect of temperature and thermodynamic properties

The adsorption behavior of BMA for diuron removal was studied at three different temperatures (303, 318, and 328 K) and concentrations ( $21.46$ – $128.76 \mu\text{mol/L}$ ). It was observed that the removal of diuron on BMA was improved with the increase in temperature. This endothermic adsorption was mainly due to the interaction between diuron and water molecules and also related to change in planarity of diuron molecule with temperature. Camara et al. [30] reported the weakening of hydrogen bonding between diuron and water molecules at higher temperatures, leading finally to dehydration. This favors the easy penetration of diuron molecules into micropores of BMA at higher temperatures. Camara et al. [30] also reported that a larger dipolar moment of diuron at higher temperatures enhanced diuron interaction with adsorbent.

The change in thermodynamic properties as described in the “Thermodynamic Properties” section was investigated for  $128.76 \mu\text{mol/L}$  concentration of

Table 5  
Characteristics of various particle-size ranges of RHA and BFA

RHA			BFA		
Particle size (mm)	BET Surface area (m <sup>2</sup> /g)	Silica-to-carbon ratio	Particle size (mm)	BET surface area (m <sup>2</sup> /g)	Silica-to-carbon ratio
<0.089	13.65	31.83	<0.104	35.50	2.02
0.089–0.152	17.92	28.58	0.104–0.178	62.58	0.86
0.152–0.251	26.25	23.60	0.178–0.251	84.85	0.29
0.251–0.354	44.37	14.76	0.251–0.354	98.08	0.12
0.354–0.500	92.08	6.02			

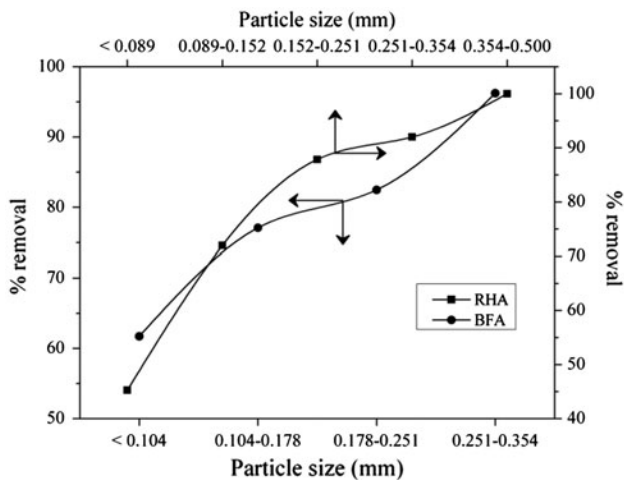


Fig. 5. Effect of particle size of RHA and BFA on the removal of diuron ( $C_0 = 85.84 \mu\text{mol/L}$ ).

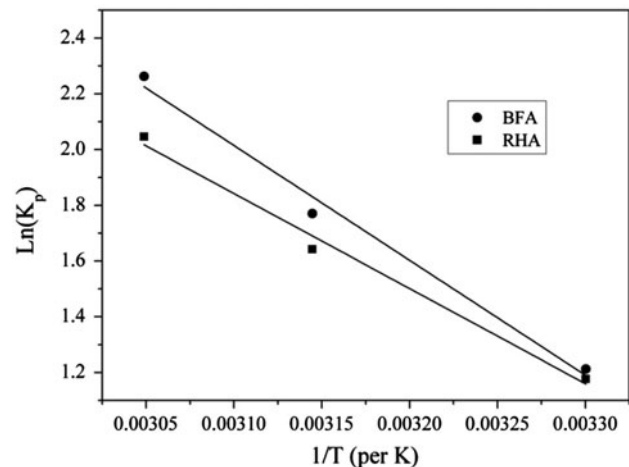


Fig. 6. Van't Hoff plot for adsorption of diuron ( $128.76 \mu\text{mol/L}$ ) on RHA and BFA.

the adsorbents using van't Hoff plot as shown in Fig. 6. Values of  $\Delta H$  (kJ/mol) and  $\Delta S$  (kJ/(mol K)) were calculated as 28.35 and 0.103 for RHA and 34.237 and 0.123 for BFA, respectively. The values of  $\Delta G$  (kJ/mol) were found to be  $-2.966$ ,  $-4.342$ , and  $-5.581$  for RHA and  $-3.054$ ,  $-4.682$ , and  $-6.170$  for BFA at three different temperatures (303, 318, and 328 K), respectively. A negative  $\Delta G$  value is the sign of feasibility and spontaneity of the adsorption process. In addition, the  $\Delta G$  value obtained in this study confirms physisorption of diuron on BMA because its value in a range of 0 to  $-20$  kJ/mol was previously reported for physisorption [31]. The reduction of  $\Delta G$  with increasing temperature indicates a decrease of spontaneity with temperature. The increased randomness at solid solution interface during adsorption is represented by positive values of  $\Delta S$ . The investigation of  $T\Delta S$  shows higher value of  $T\Delta S$  relative to  $\Delta H$ , which signifies the adsorption of diuron on BMA driven by entropy rather than enthalpy. Positive  $\Delta H$  values suggest the endothermic nature of adsorption on BMA.

### 3.7. Adsorption kinetic modeling

Experimental results were correlated with linear forms of kinetic models and rate constants along with coefficient of determination ( $R^2$ ) and error deviations, as listed in Table 6 for different initial concentrations are determined. The rate constant  $k_1$  is not linearly proportional to concentration owing to pore diffusion occurring only in the later stage of adsorption. The  $R^2$  values (0.997, 0.993, and 0.991 for BFA; and 0.978, 0.943, and 0.984 for RHA) are improved if PFO is applied for first 60 min. This confirms the applicability of PFO for rapid liquid-phase adsorption, which occurs on the BMA surface initially. However, PFO is not suitable for the entire adsorption process of diuron on either adsorbent because experimental and corresponding calculated equilibrium capacities for both adsorbents are much different in addition to lower  $R^2$  (Table 6). For the PSO model presented in Fig. 7, calculated and experimental equilibrium capacities (Table 6) are close and as a consequence,  $R^2$  values are

Table 6  
Kinetic model parameters for diuron adsorption on RHA and BFA

C <sub>0</sub> (μmol/L)	q <sub>fe,expt</sub> (μmol/g)	Pseudo-first-order model					Pseudo-second-order model							
		k <sub>1</sub> (min <sup>-1</sup> )	q <sub>fe,cal</sub> (μmol/g)	R <sup>2</sup>	ARE (%)	SSE	MPSD	k <sub>2</sub> (g/(μmol min))	q <sub>fe,cal</sub> (μmol/g)	R <sup>2</sup>	ARE (%)	SSE	MPSD	
<b>RHA</b>														
42.92	4.23	0.013	2.2727	0.893	6.610	3.831	15.424	1.058 × 10 <sup>-2</sup>	4.5	0.999	0.912	0.073	2.127	
85.84	7.57	0.007	4.0959	0.907	5.737	12.069	11.473	3.6973 × 10 <sup>-3</sup>	8	0.998	0.710	0.185	1.420	
128.76	9.96	0.012	7.5232	0.897	2.447	5.938	4.078	2.9258 × 10 <sup>-3</sup>	10.638	0.998	0.681	0.460	1.134	
<b>BFA</b>														
42.92	17.55	0.01	6.979	0.956	6.693	111.746	12.047	3.614 × 10 <sup>-3</sup>	18.18	0.999	0.399	0.396	0.718	
85.84	31.39	0.004	11.542	0.911	5.748	393.943	9.033	1.040 × 10 <sup>-3</sup>	32.258	0.999	0.251	0.753	0.395	
128.76	42.92	0.003	15.533	0.969	4.908	750.048	7.090	6.621 × 10 <sup>-4</sup>	45.454	0.999	0.454	6.423	0.656	
<b>Elovich model</b>														
C <sub>0</sub> (μmol/L)	q <sub>fe,expt</sub> (μmol/g)	α (μmol/(g min))	β (g/μmol)	R <sup>2</sup>	ARE (%)	SSE	MPSD	<b>Intraparticle diffusion model</b>						
								k <sub>di</sub> (μmol/(g min <sup>1/2</sup> ))	C <sub>1</sub> (μmol/g)	R <sup>2</sup> <sub>1</sub>	k <sub>d2</sub> (μmol/(g min <sup>1/2</sup> ))	C <sub>2</sub> (μmol/g)	R <sup>2</sup> <sub>2</sub>	D <sub>eff</sub> (cm <sup>2</sup> /min)
<b>RHA</b>														
42.92	4.23	0.7172	1.2547	0.991	2.158	0.368	7.168	0.265	1.097	0.940	0.043	3.409	0.939	3.025 × 10 <sup>-8</sup>
85.84	7.57	1.11958	0.78308	0.989	1.816	0.021	1.042	0.342	2.673	0.959	0.051	6.176	0.985	1.629 × 10 <sup>-8</sup>
128.76	9.96	1.4073	0.580	0.987	0.357	0.112	1.674	0.499	2.985	0.948	0.096	7.763	0.982	2.094 × 10 <sup>-8</sup>
<b>BFA</b>														
42.92	17.55	14.4545	0.4368	0.990	0.508	0.644	1.143	0.650	8.466	0.899	0.160	14.17	0.987	2.556 × 10 <sup>-8</sup>
85.84	31.39	59.6922	0.30854	0.997	0.036	0.015	0.066	0.750	16.60	0.991	0.266	23.43	0.989	1.022 × 10 <sup>-8</sup>
128.76	42.92	103.3962	0.23573	0.989	0.046	0.066	0.074	1.013	22.56	0.988	0.273	34.07	0.959	7.667 × 10 <sup>-9</sup>



higher than 0.99. This implies that the adsorption of diuron on BMA is governed by the PSO kinetic model, suggesting chemisorption of diuron on both adsorbents [18,32]. The kinetic constant  $k_2$  is decreased and equilibrium capacity is increased with the increase in initial concentration. The EL model applied to experimental data presents good linear fit as indicated in Fig. 8. The  $R^2$  values for the EL model are better next to that of PSO, and thus this model also supports chemisorption [33]. Fitting of the EL model is indicative of heterogeneous surface [19], which suggests the presence of active sites with different activation energies in case of BMA. The EL constants  $\alpha$  and  $\beta$  indicate the increase in adsorption rate and reduction in surface coverage with the increase in concentration. The Weber–Morris plot ( $q_t$  vs.  $t^{1/2}$ ) of the IPD model exhibited multilinearity as presented in Fig. 9 for both adsorbents, and therefore, it can be said that there exist two or more steps controlling adsorption [34]. The initial stage is instantaneous external surface adsorption or boundary layer diffusion that indicates mass transfer of diuron molecules from the liquid phase to the solid surface, and the lateral plateau of the plot is attributed to IPD representing gradual adsorption of molecules into pores [35,36]. The rate constants  $k_{d1}$  and  $k_{d2}$  (Table 6) corresponding to slopes of two stages of the plot reveal the favorable external mass transfer and IPD at high initial concentration, respectively. Furthermore, a large number of diuron molecules, before their diffusion into pores, are adsorbed on the surface due to external mass transfer, as  $k_{d1} > k_{d2}$ . The slope ( $k_{d2}$ ) of the second linear portion is used to define the IPD rate constant, whereas intercept  $C_2$  is related to boundary layer thickness.

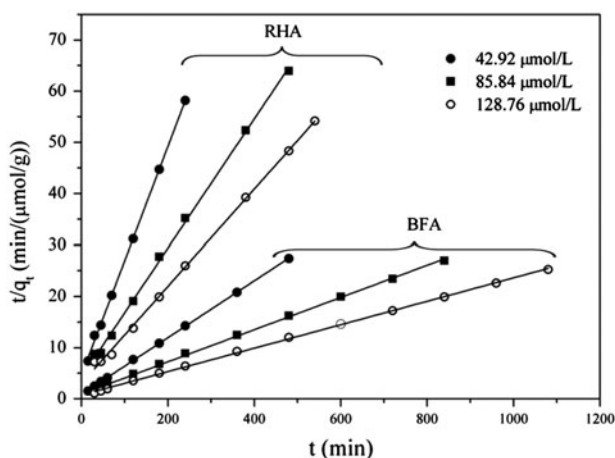


Fig. 7. Pseudo-second-order kinetic model for adsorption of diuron on RHA and BFA.

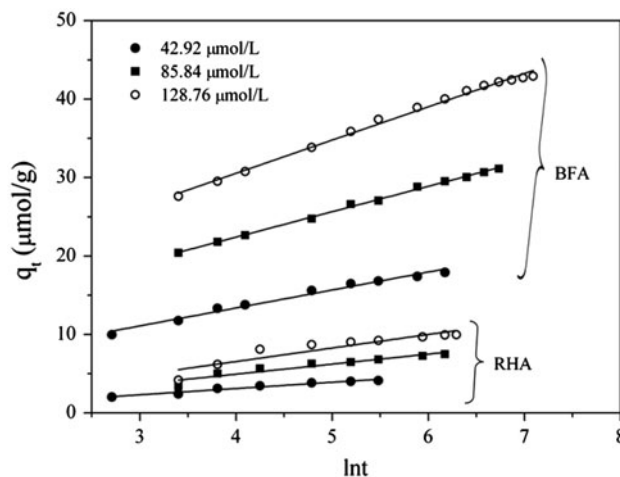


Fig. 8. Elovich kinetic model for adsorption of diuron on RHA and BFA at different initial concentrations.

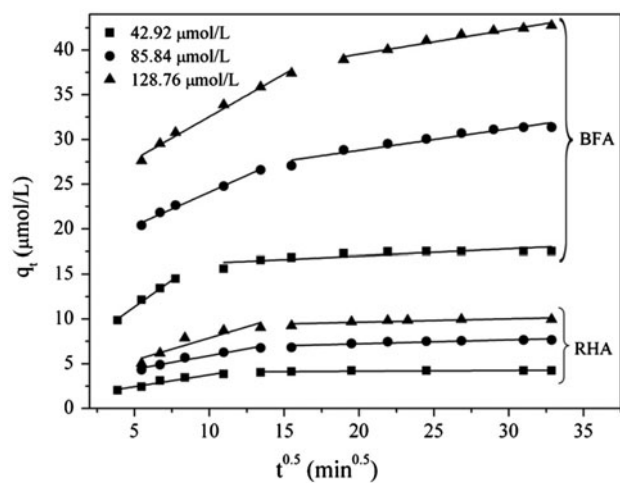


Fig. 9. Weber–Morris plot for adsorption of diuron on RHA and BFA at different initial concentrations.

The step, boundary layer or intra-particle diffusion, that governs the adsorption of diuron on RHA and BFA is determined using Boyd film diffusion model as described by Kalavathy et al. [18] and Njoku and Hameed [37]. The plot of “ $B_t$ ” (mathematical function of fractional attainment of equilibrium) vs.  $t$  is used to find the rate-limiting step in adsorption. As indicated in Fig. 1S (Supplementary Information), despite the good coefficient of determination values ( $R^2 = 0.952$ – $0.982$ ), the straight lines have nonzero intercepts (0.129–0.451) for both adsorbents, and therefore, intraparticle diffusion cannot be considered as the rate-governing step for the adsorption of diuron. The boundary layer diffusion may likely be the

rate-limiting step in adsorption [38]. The effective diffusion coefficients ( $D_{\text{eff}}$ ,  $\text{cm}^2/\text{s}$ ) are calculated from the slope of  $B_t$  vs.  $t$  plot for different initial concentrations, and the values are listed in Table 6.

To confirm this observation, a Boyd plot of  $\log(1 - F)$  vs.  $t$  (Fig. 2S, Supplementary Information) is studied at different concentrations. The intercepts of straight lines are in the range  $-0.094$  to  $-0.369$  with  $R^2$  between 0.912 and 0.964. The nonzero intercept of  $\log(1 - F)$  vs.  $t$  plot indicates that the boundary layer diffusion is not purely a rate-limiting step in diuron adsorption. Finally, it can be deduced that PSO and EL mechanisms are more likely the adsorption kinetics and both boundary layer and intraparticle diffusion participate in governing the diffusion of diuron molecules.

Among the PFO, PSO, and Elovich kinetic models, the best fitting one can be determined based on the values of error functions listed in Table 6. According to Table 6, the lower values of ARE (%), SSE, and MPSD notify that the Elovich model and pseudo-second-order kinetic model are the most appropriate models to adequately describe the adsorption of diuron on BMA.

### 3.8. Adsorption isotherm modeling

Langmuir, Freundlich, and Temkin isotherm models [39] applied to the adsorption of diuron on BMA at three different temperatures are shown in Figs. 10–12. Isotherm parameters and coefficient of determination ( $R^2$ ) with error deviations for linear regression are listed in Table 7. The Langmuir isotherm assumes monolayer adsorption on adsorbent surface with finite number of homogeneous active sites [40]. According to the Langmuir isotherm, heat of adsorption associated with active sites is constant with coverage of adsorbent surface. As indicated in Table 7, Langmuir monolayer adsorption capacity of BMA is increased with temperature. Comparatively, adsorption capacity of BFA is about 4.4 times greater than that of RHA. The increment in Langmuir constant with temperature is indicative of greater affinity for binding of diuron molecules on both adsorbents at higher temperatures. Therefore, adsorption of diuron is stronger at higher temperatures because heat of adsorption, which is proportional to Langmuir constant, is high. In addition, there is stronger adsorption of diuron on RHA at higher temperatures, compared with that on BFA. Literature report [41] suggests the use of Langmuir constant to calculate the dimensionless factor [ $R_L = 1/(1 + K_L C_0)$ ], which demonstrates the nature of adsorption. In this study, the values of  $R_L$

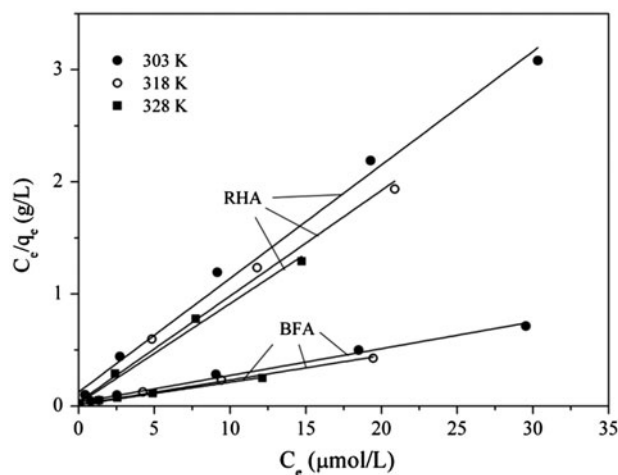


Fig. 10. Langmuir isotherm model for adsorption of diuron on RHA and BFA at different temperatures.

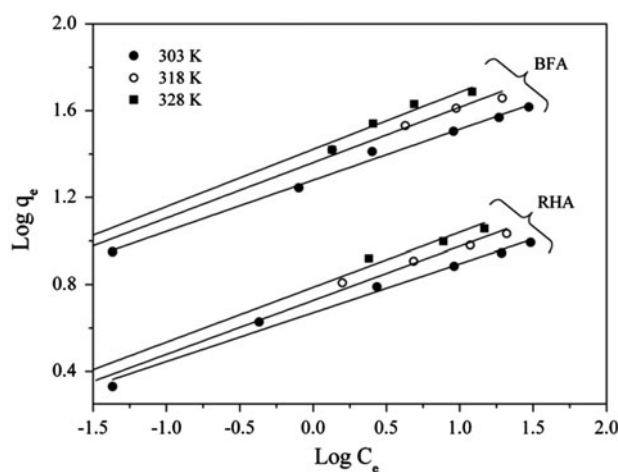


Fig. 11. Freundlich isotherm model for adsorption of diuron on RHA and BFA at different temperatures.

were found to be between 0 and 1 for all initial concentrations considered at three different temperatures. Thus, the temperature range of 303–328 K is considered to be favorable for adsorption of diuron on BMA. In contrast to the Langmuir isotherm, Freundlich isotherm is derived by assuming heterogeneous surface of adsorbent with heat of adsorption decreasing in logarithmic trend with increasing coverage [42]. Freundlich constants ( $1/n$  and  $K_F$ ) are the function of temperature as can be observed in Table 7. As with  $R_L$  for Langmuir isotherm, values of  $1/n$  for Freundlich isotherm lie between 0 and 1, which again indicates favorable adsorption of diuron on the studied adsorbents. Temkin isotherm constant  $A_T$  is related to

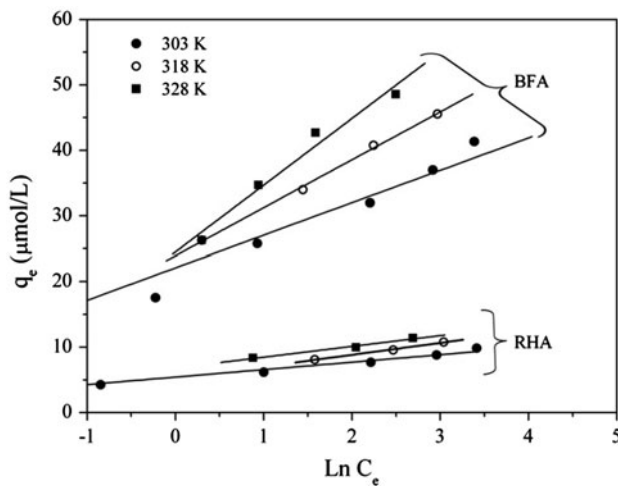


Fig. 12. Temkin isotherm model for adsorption of diuron on RHA and BFA at different temperatures.

adsorbate–adsorbent binding at equilibrium corresponding to maximum binding energy, whereas  $b_T$  is associated with heat of adsorption. The values of  $b_T$  for diuron adsorption on BMA are very low compared with that reported for ion-exchange mechanism

(8–16 kJ/mol). Similarly, adsorption energies for physisorption processes are noted to be less than  $-40$  kJ/mol. Therefore, based on  $b_T$  values (less than  $-40$  kJ/mol) described by Hu et al. [43], physisorption as well as chemisorption of diuron on both adsorbents can be proposed in this study.

It is not good enough to just compare  $R^2$  to find the best suitable isotherm, as very close values of  $R^2$  are considered for all isotherms. Therefore, the average relative error (ARE, %), the sum of the squares of the errors (SSE), and MPSD functions were used to determine and evaluate the fitting of isotherms to experimental data. Lower ARE (%), SSE, and MPSD values in Table 7 signify the applicability of Freundlich followed by Temkin isotherm to experimental data. Fitting of these two isotherms reflects the heterogeneous surface of RHA and BFA.

#### 4. Comparison between diuron adsorbents

Previous studies have reported adsorbents of different origins for diuron removal from aqueous solution as shown in Table 8. It can be seen from the table that the surface area of these adsorbents is larger than the adsorbent used in this study. However, based on

Table 7  
Isotherm parameters for diuron adsorption on RHA and BFA at different temperatures

Isotherm models	Parameters	Temperature (K)					
		303		318		328	
		RHA	BFA	RHA	BFA	RHA	BFA
Langmuir	$q_{\max}$ ( $\mu\text{mol/g}$ )	9.9	43.48	10.64	47.62	11.36	50
	$K_L$ ( $\text{L}/\mu\text{mol}$ )	0.808	0.697	2.474	1.500	3.667	1.818
	$R^2$	0.991	0.994	0.991	0.992	0.992	0.994
	ARE (%)	26.27	21.93	10.72	13.13	11.58	15.18
	SSE	8.039	108.608	3.620	96.499	4.579	133.052
	MPSD	67.383	63.018	91.080	22.146	17.453	28.438
Freundlich	$1/n$	0.225	0.235	0.198	0.209	0.169	0.277
	$K_F [(\mu\text{mol/g})/(\mu\text{mol/L})^{1/n}]$	4.677	19.011	5.875	24.888	7.144	25.586
	$R^2$	0.988	0.994	0.999	0.994	0.991	0.992
	ARE (%)	4.61	2.78	0.57	2.38	1.12	5.54
	SSE	0.412	5.922	0.009	3.229	0.044	19.487
	MPSD	9.486	6.555	0.765	2.999	1.432	7.953
Temkin	$A_T$ ( $\text{L}/\mu\text{mol}$ )	61.88	87.39	52.20	26.26	18.16	11.03
	$B$	0.319	1.152	0.404	1.705	0.384	2.376
	$b_T$ (kJ/mol)	7.893	2.187	6.549	1.551	5.996	1.148
	$R^2$	0.984	0.985	0.993	0.997	0.982	0.972
	ARE (%)	5.85	10.08	4.84	7.69	2.56	6.51
	MPSD	12.800	24.11	1.098	1.366	3.457	5.284

Table 8  
Comparison of diuron adsorption of this work with previous studies

S. no.	Adsorbent	Capacity ( $\mu\text{mol}/\text{m}^2$ )	BET surface area ( $\text{m}^2/\text{g}$ )	Refs.
1	Multiwalled carbon nanotubes	1.405	558.15	[8]
2	Multiwalled carbon nanotubes	0.657	258.6	[11]
	Oxidized multiwalled carbon nanotubes	0.4879	427.5	
3	CTA- $\text{Fe}_x(\text{OH})_y$ montm	1.244	10	[15]
		0.375	12	
4	Activated carbon fiber	1.496	1,709	[23]
	Oxidized activated carbon fiber	0.907	1,315	
5	Activated carbon	0.193	1,139	[45]
6	Activated carbon fiber	1.675	1,709	[46]
	Activated carbon cloth	1.754	2,128	
	Granular activated carbon	1.138	1,191	
7	Montmorillonite	0.021	47.20	[47]
	Montmorillonite 180	0.007	103.75	
	Montmorillonite 180 h	0.021	103.84	
	Sepiolite	0.013	248	
	Sepiolite 180	0.018	218	
	Sepiolite 180 h	0.036	167	
8	Activated carbon	1.545	776	[48]
	Wheat carbon	0.472	310	
9	Activated carbon cloth	0.530	2,128	[49]
	Activated carbon fiber	1.569	1,709	
10	BFA	0.963	51.93	This study
	RHA	0.334	33.99	

surface area, the adsorption capacity of the adsorbent used in this study (i.e. BMA) is higher than that of some of the adsorbents previously studied. This indicates that for each square meter of surface, BMA has greater potential to adsorb diuron. In addition, the adsorption capacity per gram of BMA is higher than sodium-rich fresh montmorillonite and sodium-rich modified montmorillonite (capacity 0.22–3.40  $\mu\text{mol}/\text{g}$ ) as well as calcium-rich fresh montmorillonite and calcium-rich modified montmorillonite (capacity 0.03–3.13  $\mu\text{mol}/\text{g}$ ) [16]. Moreover, BMA is better in terms of capacity than Chinese cultivated soils (capacity 0.009–0.111  $\mu\text{mol}/\text{g}$ ) [13] and activated date seed (capacity 8.586  $\mu\text{mol}/\text{g}$ ) [44]. Therefore, from a cost, availability, and capacity point of view, BMA can be considered an efficient adsorbent for removal of diuron.

## 5. Conclusion

Our study results show that BMAs are efficient adsorbent for diuron removal. Because of higher carbon content and larger BET surface area, BFA exhibited greater adsorption capacity, compared with RHA. The uptake capacity of BFA and RHA is higher than natural adsorbents such as soil and comparable with

activated carbon/multiwalled carbon nanotubes. Owing to higher pore diameter, RHA gave faster pore adsorption in the later stages. In the initial stage, however, due to greater external surface area and boundary layer diffusion coefficient, higher kinetics of adsorption was observed for BFA. When the uptake capacity of BFA and RHA for the same size fraction is compared, it was found that BFA has four times higher capacity than RHA, which indicates that BFA has more active sites apart from having two times higher surface area. Because diuron exists in the molecular form at  $\text{pH} > 6$ , adsorption follows a non-electrostatic mechanism, which was similar to that observed in the literature.

## Supplementary material

The supplementary material for this paper is available online at <http://dx.doi.org/10.1080/19443994.2015.1132394>.

## Acknowledgments

We thank the Science and Engineering Research Board (SERB), India, for providing us a research grant (Grant No. SB/S3/CE/077/2013) to undertake this

work. Sophisticated characterization facilities provided by IBM, Nagpur, India, and CSMCRI, Bhavnagar, India, are gratefully acknowledged. The authors also thank Dr Sayaji Mehtre, Scientist BARC, Mumbai, India, for his assistance in characterization studies.

## Nomenclature

The following symbols were used in this paper

$k_1$	— pseudo-first-order kinetic constant ( $\text{min}^{-1}$ )
$k_2$	— pseudo-second-order kinetic constant ( $\text{g}/(\mu\text{mol min})$ )
$\beta$	— constant related extent of surface coverage and activation energy ( $\text{g}/\mu\text{mol}$ )
$\alpha$	— initial sorption rate ( $\mu\text{mol}/(\text{g min})$ )
$k_d$	— intra-particle diffusion rate constant ( $\mu\text{mol}/(\text{g min}^{1/2})$ )
$C$	— intercept related to thickness of boundary layer ( $\mu\text{mol}/\text{g}$ )
$D_{\text{eff}}$	— effective diffusion coefficient ( $\text{cm}^2/\text{min}$ )
$K_L$	— Langmuir constants ( $\text{L}/\mu\text{mol}$ )
$q_{\text{max}}$	— Langmuir adsorption capacity ( $\mu\text{mol}/\text{g}$ )
$K_F$	— Freundlich constant ( $(\mu\text{mol}/\text{g})/(\mu\text{mol}/\text{L})^{1/n}$ )
$n$	— intensity of adsorption
$b_T$	— Temkin isotherm energy constant ( $\text{J}/\text{mol}$ )
$A_T$	— equilibrium binding constant ( $\text{L}/\mu\text{mol}$ )
$\Delta H$	— change in enthalpy ( $\text{kJ}/\text{mol}$ )
$\Delta G$	— Gibbs free energy change
$\Delta S$	— entropy change ( $\text{kJ}/(\text{mol K})$ )
$R$	— universal gas constant ( $8.314 \text{ J}/(\text{mol K})$ )

## References

- [1] Ministry of agriculture, Economics and statistics, Government of India, Agriculture statistics at a glance 2014. Available from: <[http://eands.dacnet.nic.in/lat\\_est\\_2006.htm](http://eands.dacnet.nic.in/lat_est_2006.htm)> (Date of access: 20 January 2014).
- [2] R. Khan, A. Jabbar, I. Ahmad, W. Khan, A.N. Khan, J. Mirza, Reduction in environmental problems using rice-husk ash in concrete, *Constr. Build. Mater.* 30 (2012) 360–365.
- [3] T. Akram, S.A. Memon, H. Obaid, Production of low cost self compacting concrete using bagasse ash, *Constr. Build. Mater.* 23 (2009) 703–712.
- [4] K.Y. Foo, B.H. Hameed, Utilization of rice husk ash as novel adsorbent: A judicious recycling of the colloidal agricultural waste, *Adv. Colloid Interface Sci.* 152 (2009) 39–47.
- [5] M. Ahmaruzzaman, V.K. Gupta, Rice husk and its ash as low-cost adsorbents in water and wastewater treatment, *Ind. Eng. Chem. Res.* 50 (2011) 13589–13613.
- [6] M. Ahmaruzzaman, A review on the utilization of fly ash, *Prog. Energy Combust. Sci.* 36 (2010) 327–363.
- [7] V.K. Gupta, C.K. Jain, I. Ali, S. Chandra, S. Agarwal, Removal of lindane and malathion from wastewater using bagasse fly ash—a sugar industry waste, *Water Res.* 36 (2002) 2483–2490.
- [8] G.C. Chen, X.Q. Shan, Z.G. Pei, H. Wang, L.R. Zheng, J. Zhang, Y.N. Xie, Adsorption of diuron and dichlobenil on multiwalled carbon nanotubes as affected by lead, *J. Hazard. Mater.* 188 (2011) 156–163.
- [9] S. Baup, D. Wolbert, A. Laplanche, Importance of surface diffusivities in pesticide adsorption kinetics onto granular versus powdered activated carbon: Experimental determination and modeling, *Environ. Technol.* 23 (2002) 1107–1117.
- [10] G. Kyriakopoulos, D. Doulia, Adsorption of pesticides on carbonaceous and polymeric materials from aqueous solutions: A Review, *Sep. Purif. Rev.* 35 (2006) 97–191.
- [11] K. Sun, Z. Zhang, B. Gao, Z. Wang, D. Xu, J. Jin, X. Liu, Adsorption of diuron, fluridone and norflurazon on single-walled and multi-walled carbon nanotubes, *Sci. Total Environ.* 439 (2012) 1–7.
- [12] J. Deng, Y. Shao, N. Gao, Y. Deng, C. Tan, S. Zhou, X. Hu, Multiwalled carbon nanotubes as adsorbents for removal of herbicide diuron from aqueous solution, *Chem. Eng. J.* 193–194 (2012) 339–347.
- [13] Y. Liu, Z. Xu, X. Wu, W. Gui, G. Zhu, Adsorption and desorption behavior of herbicide diuron on various Chinese cultivated soils, *J. Hazard. Mater.* 178 (2010) 462–468.
- [14] J.D. Fernández-Bayo, R. Nogales, E. Romero, Evaluation of the sorption process for imidacloprid and diuron in eight agricultural soils from Southern Europe using various kinetic models, *J. Agric. Food Chem.* 56 (2008) 5266–5272.
- [15] O. Bouras, J.C. Bollinger, M. Baudu, H. Khalaf, Adsorption of diuron and its degradation products from aqueous solution by surfactant-modified pillared clays, *Appl. Clay Sci.* 37 (2007) 240–250.
- [16] R. Celis, C. Trigo, G. Facenda, M.C. Hermosín, J. Cornejo, Selective modification of clay minerals for the adsorption of herbicides widely used in olive groves, *J. Agric. Food Chem.* 55 (2007) 6650–6658.
- [17] Indian standard methods of test for coal and coke, IS: 1350 (Part 1), Methods of test for coal and coke, proximate analysis, Bureau of Indian Standards, Manak Bhawan, New Delhi, India.
- [18] M. Kalavathy, T. Karthikeyan, S. Rajgopal, L.R. Miranda, Kinetic and isotherm studies of Cu(II) adsorption onto  $\text{H}_3\text{PO}_4$ -activated rubber wood sawdust, *J. Colloid Interface Sci.* 292 (2005) 354–362.
- [19] P.D. Pathak, S.A. Mandavgane, B.D. Kulkarni, Utilization of banana peel for the removal of benzoic and salicylic acid from aqueous solutions and its potential reuse, *Desalin. Water Treat.* 1–13 (2015), doi: [10.1080/19443994.2015.1051589](https://doi.org/10.1080/19443994.2015.1051589).
- [20] S. Sadaf, H.N. Bhatti, S. Ali, K. Rehman, Removal of Indosol Turquoise FBL dye from aqueous solution by bagasse, a low cost agricultural waste: Batch and column study, *Desalin. Water Treat.* 52 (2014) 184–198.
- [21] S.K. Deokar, S.A. Mandavgane, B.D. Kulkarni, Behaviour of biomass multicomponent ashes as adsorbents, *Curr. Sci.* (in press).
- [22] M.A. Hanif, H.N. Bhatti, Remediation of heavy metals using easily cultivable, fast growing, and highly accumulating white rot fungi from hazardous aqueous streams, *Desalin. Water Treat.* 53 (2015) 238–248.
- [23] M.A.F. Camara, M.V.L. Ramon, M.A.A. Merino, C.M. Castilla, Effect of surface chemistry, solution pH, and ionic strength on the removal of herbicides diuron and amitrole from water by an activated carbon fiber, *Langmuir* 23 (2007) 1242–1247.
- [24] V.C. Srivastava, I.D. Mall, I.M. Mishra, Characterization of mesoporous rice husk ash (RHA) and adsorption kinetics of metal ions from aqueous solution onto RHA, *J. Hazard. Mater.* 134 (2006) 257–267.

- [25] D.H. Lataye, I.M. Mishra, I.D. Mall, Adsorption of 2-picoline onto bagasse fly ash from aqueous solution, *Chem. Eng. J.* 138 (2008) 35–46.
- [26] V.K. Gupta, D. Mohan, Suhas, K.P. Singh, Removal of 2-aminophenol using novel adsorbents, *Ind. Eng. Chem. Res.* 45 (2006) 1113–1122.
- [27] V.K. Gupta, A. Mittal, L. Krishnan, J. Mittal, Adsorption treatment and recovery of the hazardous dye, Brilliant Blue FCF, over bottom ash and de-oiled soya, *J. Colloid Interface Sci.* 293 (2006) 16–26.
- [28] S.K. Deokar, S.A. Mandavgane, Estimation of packed-bed parameters and prediction of breakthrough curves for adsorptive removal of 2,4-Dichlorophenoxyacetic acid using rice husk ash, *J. Environ. Chem. Eng.* 3 (2015) 1827–1836.
- [29] W.T. Tsai, C.W. Lai, K.J. Hsien, Effect of particle size of activated clay on the adsorption of paraquat from aqueous solution, *J. Colloid Interface Sci.* 263 (2003) 29–34.
- [30] M.A.F. Camara, M.V.L. Ramon, M.A.A. Merino, C.M. Castilla, About the endothermic nature of the adsorption of the herbicide diuron from aqueous solutions on activated carbon fiber, *Carbon* 44 (2006) 2335–2338.
- [31] C.Y. Kuo, C.H. Wu, J.Y. Wu, Adsorption of direct dyes from aqueous solutions by carbon nanotubes: Determination of equilibrium, kinetics and thermodynamics parameters, *J. Colloid Interface Sci.* 327 (2008) 308–315.
- [32] H. Cui, Q. Li, Y. Qian, Q. Zhang, J. Zhai, Preparation and adsorption performance of MnO<sub>2</sub>/PAC composite towards aqueous glyphosate, *Environ. Technol.* 33 (2012) 2049–2056.
- [33] K.D. Belaid, S. Kacha, M. Kameche, Z. Derriche, Adsorption kinetics of some textile dyes onto granular activated carbon, *J. Environ. Chem. Eng.* 1 (2013) 496–503.
- [34] R.R. Sheha, A.A. El-Zahhar, Synthesis of some ferromagnetic composite resins and their metal removal characteristics in aqueous solutions, *J. Hazard. Mater.* 150 (2008) 795–803.
- [35] J.M. Salman, B.H. Hameed, Adsorption of 2,4-dichlorophenoxyacetic acid and carbofuran pesticides onto granular activated carbon, *Desalination* 256 (2010) 129–135.
- [36] G.L. Dotto, J.A.V. Costa, L.A.A. Pinto, Kinetic studies on the biosorption of phenol by nanoparticles from *Spirulina* sp. LEB 18, *J. Environ. Chem. Eng.* 1 (2013) 1137–1143.
- [37] V.O. Njoku, B.H. Hameed, Preparation and characterization of activated carbon from corncob by chemical activation with H<sub>3</sub>PO<sub>4</sub> for 2,4-dichlorophenoxyacetic acid adsorption, *Chem. Eng. J.* 173 (2011) 391–399.
- [38] S. Ozcan, A. Tor, M.E. Aydin, An investigation on the sorption behaviour of montmorillonite for selected organochlorine pesticides from water, *Environ. Technol.* 33 (2012) 1239–1245.
- [39] N. Asasian, T. Kaghazchi, A comparison on efficiency of virgin and sulfurized agro-based adsorbents for mercury removal from aqueous systems, *Adsorption* 19 (2013) 189–200.
- [40] A. Cougnaud, C. Faur, P. Le Cloirec, Removal of pesticides from aqueous solution: Quantitative relationship between activated carbon characteristics and adsorption properties, *Environ. Technol.* 26 (2005) 857–866.
- [41] A. Kamari, S.N.M. Yusoff, F. Abdullah, W.P. Putra, Biosorptive removal of Cu(II), Ni(II) and Pb(II) ions from aqueous solutions using coconut dregs residue: Adsorption and characterisation studies, *J. Environ. Chem. Eng.* 2 (2014) 1912–1919.
- [42] D. Ova, B. Ovez, 2,4-Dichlorophenoxyacetic acid removal from aqueous solutions via adsorption in the presence of biological contamination, *J. Environ. Chem. Eng.* 1 (2013) 13–21.
- [43] X. Hu, J. Wang, Y. Liu, X. Li, G. Zeng, Z. Bao, X. Zeng, A. Chen, F. Long, Adsorption of chromium(VI) by ethylenediamine-modified cross-linked magnetic chitosan resin: Isotherms, kinetics and thermodynamics, *J. Hazard. Mater.* 185 (2011) 306–314.
- [44] Y.S. Al-Degs, A.H. El-Sheikh, S.T. Jaber, Application of heated date seeds as a novel extractant for diuron from water, *Arabian J. Chem.* 6 (2013) 121–129.
- [45] M.A. Bahri, L. Calvo, J. Lemus, M.A. Gilarranz, J. Palomar, J.J. Rodriguez, Mechanistic understanding of the behavior of diuron in the adsorption from water onto activated carbon, *Chem. Eng. J.* 198–199 (2012) 346–354.
- [46] M.V.L. Ramon, M.A.F. Camara, M.A.A. Merino, C.M. Castilla, Removal of diuron and amitrole from water under static and dynamic conditions using activated carbons in form of fibers, cloth, and grains, *Water Res.* 41 (2007) 2865–2870.
- [47] C. Maqueda, M. dos Santos Afonso, E. Morillo, R.M. Torres Sánchez, M. Perez-Sayago, T. Undabeytia, Adsorption of diuron on mechanically and thermally treated montmorillonite and sepiolite, *Appl. Clay Sci.* 72 (2013) 175–183.
- [48] Y. Yang, Y. Chun, G. Sheng, M. Huang, pH-dependence of pesticide adsorption by wheat-residue-derived black carbon, *Langmuir* 20 (2004) 6736–6741.
- [49] M.A.F. Camara, M.V.L. Ramon, M.A.A. Merino, C.M. Castilla, Temperature dependence of herbicide adsorption from aqueous solutions on activated carbon fiber and cloth, *Langmuir* 22 (2006) 9586–9590.